In situ monitoring of second-harmonic generation in human corneas to compensate for femtosecond laser pulse attenuation in keratoplasty

Valeria Nuzzo
Karsten Plamann
Laboratoire d'Optique Appliquée
ENSTA-École Polytechnique-CNRS UMR 7639
Chemin de la Hunière
91761 Palaiseau Cedex, France
and
Laboratoire Biotechnologie et Œil
Université René Descartes
Paris V, EA 4063
Hôpital Hôtel Dieu
1 place du parvis Notre Dame
75181 Paris Cedex 4, France
E-mail: valeria.nuzzo@polytechnique.edu

Michèle Savoldelli
Université René Descartes
Laboratoire Biotechnologie et Œil
Paris V, EA 4063 France
and
Hôpital Hôtel Dieu
1 place du parvis Notre Dame
75181 Paris Cedex 4, France

Michele Merano
Ecole Nationale Supérieure de Techniques Avancées
CNRS UMR 7639
Laboratoire d'Optique Appliquée
Chemin de la Hunière
91761 Palaiseau Cedex, France

David Donate
Université René Descartes
Laboratoire Biotechnologie et Œil
Paris V, EA 4063 France
and
Hôpital Hôtel Dieu
1 place du parvis Notre Dame
75181 Paris Cedex 4, France

Olivier Albert
Pedro Felipe Gardeazábal Rodríguez
Ecole Nationale Supérieure de Techniques Avancées
CNRS UMR 7639
Laboratoire d'Optique Appliquée
Chemin de la Hunière
91761 Palaiseau Cedex, France
and
Université René Descartes
Laboratoire Biotechnologie et Œil
Paris V, EA 4063 France
and
Hôpital Hôtel Dieu
1 place du parvis Notre Dame
75181 Paris Cedex 4, France

Gerard Mourou
Ecole Nationale Supérieure de Techniques Avancées
CNRS UMR 7639
Laboratoire d'Optique Appliquée
Chemin de la Hunière
91761 Palaiseau Cedex, France

Jean-Marc Legeais
Université René Descartes
Laboratoire Biotechnologie et Œil
Paris V, EA 4063 France
and
Hôpital Hôtel Dieu
1 place du parvis Notre Dame
75181 Paris Cedex 4, France

Abstract. The application of femtosecond lasers in corneal transplant surgery requires high pulse energies to compensate for the strong optical scattering in pathological corneas. However, excessive energies deteriorate the quality of the incisions. The aim of this study is to demonstrate the dependence of side effects on local radiant exposure, numerical aperture, and tissue properties, to quantify the penetration depth of the laser for individual corneas, and to provide a method for optimizing the energy in the volume of the cornea. We examine histological and ultrastructural sections of clear and edematous corneas with perforating and lamellar incisions performed at different pulse energies. We demonstrate that the augmented energies in edematous corneas may result in unwanted side effects even when using high numerical apertures. The dependence of the laser beam penetration depth on pulse energy is evaluated by histology and an exponential decrease is observed. We show that the penetration length can be determined by evaluating the backscattered second-harmonic emission associated with the nonlinear optical properties of the tissue. This approach represents a noninvasive method for the *in situ* quantification of the laser beam attenuation, enabling us to adapt the pulse energy accordingly. Experiments using adapted energies show that the side effects are minimized.
[DOI: 10.1117/1.2811951]

Keywords: femtosecond laser eye surgery; second-harmonic generation; cornea; keratoplasty.

Paper 06300RRR received Oct. 25, 2006; revised manuscript received Aug. 21, 2007; accepted for publication Aug. 21, 2007; published online Nov. 16, 2007.

1 Introduction

Keratoplasty is referred to as corneal transplantation; it can be carried out as a total grafting (penetrating keratoplasty) or a partial grafting of the tissue (lamellar keratoplasty). The latter can be performed as an anterior keratoplasty, which addresses

Address all correspondence to Valeria Nuzzo, Laboratoire d'Optique Appliquée, ENSTA-Ecole, Polytechnique - CNRS UMR 7639, chemin de la Hunière-Palaiseau Cedex, Essonne 91761 France; Tel.: +33169319790; Fax: +330169319996; E-mail: valeria.nuzzo@ensta.fr

1083-3668/2007/12(6)/064032/11/$25.00 © 2007 SPIE

the corneal stroma, or a posterior keratoplasty during which the endothelium is replaced. Indications for keratoplasty are stromal diseases or opacity. During the last decade, an average of about 35,000 corneal transplants per year was performed in the United States and about 30,000 in the European Union.

The common surgical techniques are critical and not always reproducible considering the depth of the incisions and the difficulty in dimensioning the donor graft to match exactly the geometry of the corneal disc to be replaced in the recipient eye. These techniques are all manual or semiautomated by the use of surgical microkeratomes, which are delicate to manipulate. The potentially very high reproducibility of the femtosecond laser procedure can prevent surgery and postsurgery complications.

The first clinical (and commercial) application of femtosecond lasers in ophthalmology has been their use in a part of the laser *in situ* keratomileusis (LASIK) procedure.[1,2] LASIK is a surgical technique for the treatment of refractive errors and involves the use of a mechanical microkeratome to create a corneal flap. During surgery, the flap is opened, and the excimer laser is used to reshape the corneal tissue to correct focusing errors. The flap is subsequently replaced, enabling a rapid recovery of the patient as the optical surface of the cornea remains intact. In refractive surgery, femtosecond lasers have been shown to provide an interesting alternative to the mechanical microkeratome for the cut of the corneal flap. Compared to corneal cut with microkeratomes, no additional complications were observed, the geometrical parameters of the flap were better predicted, and the standard deviation of cut thickness was halved.[3,4]

The possibility of performing lamellar incisions in the volume of the cornea represents one of the major advantages of the femtosecond laser over mechanical techniques. In previously published studies, femtosecond laser incisions and trephinations in the cornea for posterior lamellar keratoplasty were accomplished on human corneas.[5,6] Energies up to three to four times the threshold energy for disruption at the surface of healthy corneal tissue were required.

Attenuation of the radiant exposure in the tissue is chiefly attributed to scattering and spherical aberration.[7]

1. Edema and other irregularities that are present in the patient cornea broaden and attenuate the laser beam by light scattering.

2. The greater working depth in the cornea combined with high-numerical-aperture focusing optics result in spherical aberrations that broaden the point spread function when focusing from air into the cornea as a medium with a higher refractive index.

3. Irregularities of the corneal surface (for instance in case of keratoconus) are likely to cause additional optical aberrations resulting in a further broadening of the beam and a reduction of the radiant exposure.

All the preceding mechanisms result in a larger spot size than would theoretically correspond to the numerical aperture of the focusing optics, which may increase unwanted side effects.[8]

In principle, a reduced radiant exposure can be compensated for by increasing the pulse energy sufficiently to ensure that the irradiance threshold for optical breakdown is reached in the volume of the cornea. However, at the intermediate numerical apertures of 0.3 to 0.5, typically used in clinical practice, pulse energies for optical breakdown correspond to peak powers of a few megawatts and are just below the critical energy for filamentation effects, which result from an interplay between self-focusing and defocusing by the plasma.[9,10] In the presence of filamentation, a precise local deposition of the energy in the tissue is made difficult, the predominantly deterministic and nonthermal nature of the interaction process is altered and the quality and reproducibility of the surgery is reduced.[11] To keep these effects at a low level, care must be taken not to expose the tissue to too high energies. It is therefore necessary to evaluate the attenuation of the beam in the cornea prior to surgery to adjust the pulse energy to the depth of the treatment.

To illustrate the side effects of high pulse energies, we first show histological and ultrastructural analyses of perforating incisions performed at constant energy in clear human corneas. We then examine incisions in edematous corneas to demonstrate the attenuation of the radiant exposure in the volume and to relate the quality of the incisions to the pulse energy, numerical aperture, incision depth, and contribution of scattering and spherical aberrations. Lamellar incisions were performed at varying numerical apertures to illustrate side effects caused by self-focusing. We finally use the measurement of the second-harmonic signal emitted by the cornea to quantify the attenuation constant and to optimize the laser energy, allowing for the modified properties of the tissue.

1.1 *Femtosecond Laser Technology and Laser-Tissue Interaction*

The introduction of the chirped pulse amplification technique by Strickland and Mourou[12] in 1985 and the subsequent increase in available femtosecond laser pulse energies triggered important new developments in ultrafast pulsed laser technologies and their applications. Most laboratory laser systems are based on titanium-doped sapphire as the laser material,[13] which presents a large gain bandwidth, enabling the generation of very short pulses and good thermal conductivity, reducing thermal effects even for high laser powers and intensities. Ti:sapphire are generally pumped by argon or frequency-doubled Nd:YAG lasers. In parallel to the development and improvement of Ti:sapphire lasers, the progress in laser diode technology gave rise to the development of diode-pumped femtosecond lasers. Despite their slightly less spectacular performance with respect to pulse duration and energy, these are more adapted to commercial applications due to their moderate cost and compactness. Among these, the characteristics of neodymium- or ytterbium-doped glass lasers[14] were soon considered interesting for applications in ophthalmic surgery, particularly in the cornea. Recently, fiber lasers have started to be used in femtosecond corneal surgery.

Current research addresses many aspects of the interaction of femtosecond laser radiation with matter. Below the threshold irradiance for optical breakdown of the material, nonlinear processes occur that can be used for multiphoton and nonlinear imaging. At higher radiant exposures, alterations can be induced in the material, resulting, for instance, in a local modification of the refractive index. Above the threshold for optical breakdown, precision machining is achieved as a result of the nonthermal nature of the interaction. At extreme

irradiations, high-order harmonics, secondary radiation, or particle beams can be created.

The interaction process of short pulses with tissue has been the subject of many investigations.[15–17] A detailed review of the disruption mechanism induced by femtosecond lasers was published by Vogel et al.[18] In the femtosecond regime, *a priori* two competing mechanisms contribute to the creation of free electrons: multiphoton absorption and tunneling followed by avalanche ionization.[19–23] The transition irradiance to pass from the multiphoton to tunneling ionization is of the order of 10^{13} W/cm^2, which corresponds to the typical parameters used for femtosecond corneal surgery. At time scales below a few picoseconds, acoustic and thermal relaxation phenomena can be neglected. The free electrons communicate their energy to the tissue by locally elevating the temperature via collision and recombination processes and thereby create a highly localized tensile stress. Whenever this tensile stress exceeds the critical tension for mechanical breakdown, a cavitation bubble is formed. Below the threshold for bubble formation, chemical effects likely alter the tissue: changes of the water molecules may liberate reactive oxygen species, which modify these molecules directly by resonant electron-molecule scattering.[18]

Below-irradiance values, which cause permanent modifications of the material, we can observe nonlinear optical effects. In fact, the collagen matrix constituting the cornea has been shown to have strong nonlinear optical susceptibilities, permitting the generation of frequency-doubled light under the action of short laser pulses.[24] This phenomenon is called second-harmonic generation (SHG). It occurs in highly polarizable material with a noncentrosymmetric molecular organization at the focusing volume, and its intensity grows with the square of the incident intensity. While the generated second-harmonic wave propagates predominantly in the forward direction, scattering materials such as pathological corneal tissue can enable its observation in the backward direction and thereby enable its measurement in an *in situ/in vivo* geometry.[25–27] Until now, SHG in tissues has most often been exploited in microscopy for high-resolution imaging of tissue structures and functions and to resolve the organization of collagen fibers in corneal stroma and sclera.[28–32] Compared to terawatt per square centimeter irradiances necessary for the disruption mechanism described in the following, nonlinear optical effects can be produced at megawatt to gigawatt per square centimeter irradiances, thus representing a noninvasive monitoring system resulting from the surgical laser beam itself.

2 Materials and Methods

2.1 *Laser Systems and Experimental Setup*

Figure 1 shows the experimental setup. The laser consists of a mode-locked diode-pumped neodymium:glass oscillator, followed by a chirped pulse amplification (CPA) system with a regenerative amplifier. The system delivers pulses with durations of about 500 fs at a repetition rate of 10 kHz and a central wavelength of 1.06 μm. The output energy can be adjusted by a computer-controlled attenuator up to a maximum energy of 6 μJ. The stability of the pulses had peak-to-peak fluctuations of less than 1%. Additional experiments were performed using an amplified mode-locked titanium-doped sapphire laser emitting pulses at a central wavelength of 800 nm and a repetition rate of 1 kHz with pulse durations of about 150 fs and a maximum pulse energy of 10 μJ. Delivered energies were measured with an estimated precision of about 10%.

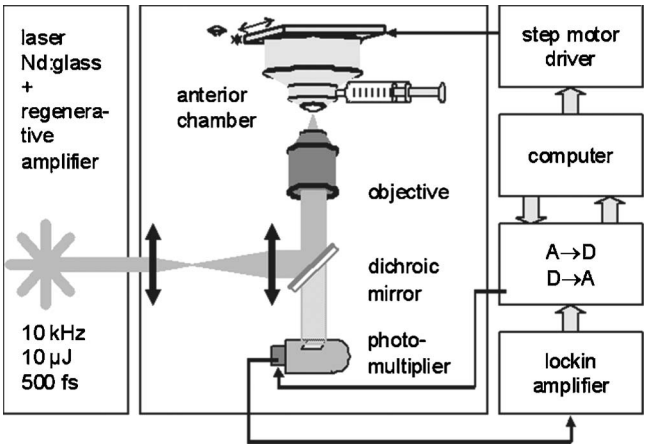

Fig. 1 Experimental setup.

The laser beam passes through a beam expander, is reflected by a dichroic mirror, and overfills the back aperture of the optics, which focus it onto the sample. The specimen is mounted onto an artificial chamber, which can be positioned in three dimensions by step motors with submicrometric resolution. Backscattered photons generated by the nonlinear laser-tissue interaction are collected by a photomultiplier positioned behind the dichroic mirror. The electronic output of the photomultiplier is filtered by a lock-in amplifier tuned to the laser repetition rate. A personal computer enables the positioning of the sample, the acquisition of nonlinear signals, and their analysis via an analog-to-digital interface.

2.2 *Sample Preparation and Experimental Protocol*

The experiments were performed on human corneas unsuitable for transplantation obtained from the Banque Française des Yeux (French Eye Bank). The corneas were stored in CorneaMax® solution until experimentations. The corneas were left in the solution for different durations to develop different degrees of edema. Each cornea was mounted on an artificial chamber filled with a physiological saline solution to reproduce natural eye hydration and pressure conditions. The epithelium was then removed with a methylcellulose spear and the cornea was flattened using a standard microscope coverslip.

Perpendicular and lamellar incisions were performed using varying pulse energies and different focusing optics with numerical apertures of 0.15, 0.3, 0.5, and 0.75 (Melles Griot achromat lens with $f=50$ mm and microscope objectives Olympus UPLFL 10×, 20×, and 40×, respectively) (Table 1). Additional experiments were performed at a numerical aperture NA of 0.6 with a focusing objective that corrects spherical aberrations at the focal point (Zeiss LD Plan-Neofluar 40×/corr.). The nondestructive measurements of the second-harmonic emission were obtained using a microscope objective (Olympus UPLFL 20×) with a numerical aperture

Table 1 Overview: parameters depending on the focusing optics.

	Coverslip Correction	NA	Airy Radius	Theoretical Threshold Energy	Experimental Threshold Energy	Strehl Ratio in Cornea (Experimental)
Melles Griot laser-grade precision-optimized achromat LAL013, f=50 mm*	—	0.15	4.1 μm	1.2 μJ	2.0(2) μJ	≥0.6(1)
Microscope objective Olympus UPLFL 10×**	—	0.3	1.6 μm	166 nJ	280(30) nJ	≥0.6(1)
Microscope objective Olympus UPLFL 20×**	170 μm	0.5	0.98 μm	59 nJ	130(20) nJ	≥0.46(5)
Microscope objective Olympus UPFL 40×**	170 μm	0.75	0.65 μm	26 nJ	60(6) nJ	≥0.44(5)
Microscope objective Zeiss LD Plan-Neofluar 40×/corr.**	170 μm	0.6	0.81 μm	41 nJ	170(15) nJ	≥0.24(3)

*λ=1.06 μm, **λ=800 nm

of 0.3. The optics used presented the necessary correction for the coverslip thickness at higher numerical apertures.

2.3 *Histological and Ultrastructural Analysis*

After the experiments, a 1-h waiting time enabled complete resorption of cavitation bubbles. The corneas were then fixed for 2 h in 2.5% glutaraldehyde in 0.1 M cacodylate buffer (pH 7.3), washed with the same buffer solution, after fixing in 0.1% osmium tetroxide and dehydrating in alcohol with graded concentrations, and finally embedded in LX 112 resin. Subsequent semithin and ultrathin sections were obtained using an ultramicrotome (Reichert OmU2). Semithin sections were stained with toluidine blue and analyzed by optical microscopy (Zeiss Phomi2), while ultrathin sections were colored by uranyl acetate and lead citrate solutions and examined with a transmission electron microscope (Philips CM10, resolution 5 Å).

3 Results

3.1 *Threshold Considerations*

The focusing optics producing the lowest NA in this study was an achromatic doublet lens (Melles Griot, LAL013, f =50 mm). Design data for this achromat was available and numerical calculations computed with an optical design code[33] (ZEMAX EE) showed that it produces a print spread function (PSF) corresponding to NA=0.15, reasonably close to a well-corrected system (Strehl ratio ≈0.7).

Following theoretical and experimental data from the literature, for pulse durations used in this study the radiant exposure threshold*,[34] is expected[2,17,18,35–37] to be just under 2 J/cm. This translates to theoretical threshold pulse energy of 1.2 μJ when assuming a diffraction-limited beam. In our experiments, consistent bubble formation was observed throughout the volume of the cornea at pulse energies of about 2±0.2 μJ. The quotient of these values delivers an experimental Strehl ratio greater than 0.6, which agrees well with the result of the preceding numerical modeling.

For the focusing optics with NA=0.3, 0.5, 0.75, and 0.6 (objectives Olympus UPLFL 10×, 20×, 40×, and Zeiss LD Plan-Neofluar 40×/corr. respectively), no design data were available. Experimental thresholds were observed at 280, 130, 60, and 170 nJ, respectively, when working close to the surface, which would correspond to 0.6±0.1, 0.46±0.05, 0.44±0.05, and 0.24±0.03 for the minimal Strehl ratios. Note that these values represent lower boundaries for the real Strehl ratios. The deviation from ideal values may be attributed to a nonuniform wavefront at the back pupil of the objectives—to which high-NA optics are particularly sensitive—and to aberrations intrinsic to the experimental setup, rather than the optical elements themselves.

*The values for the threshold radiant exposure found in the literature correspond to pulse energies divided by the surface encircled by the $1/e^2$ beam radius (for Gaussian beams) or the surface corresponding to the Airy radius. To be consistent with the published data, here we refer to the same principle of normalization. However, it has been noted that to be able to compare measured to theoretically predicted data, the peak value of the beam profile must be used, which in the case of a diffraction-limited beam is about 4 times higher than the value averaged over the Airy radius.

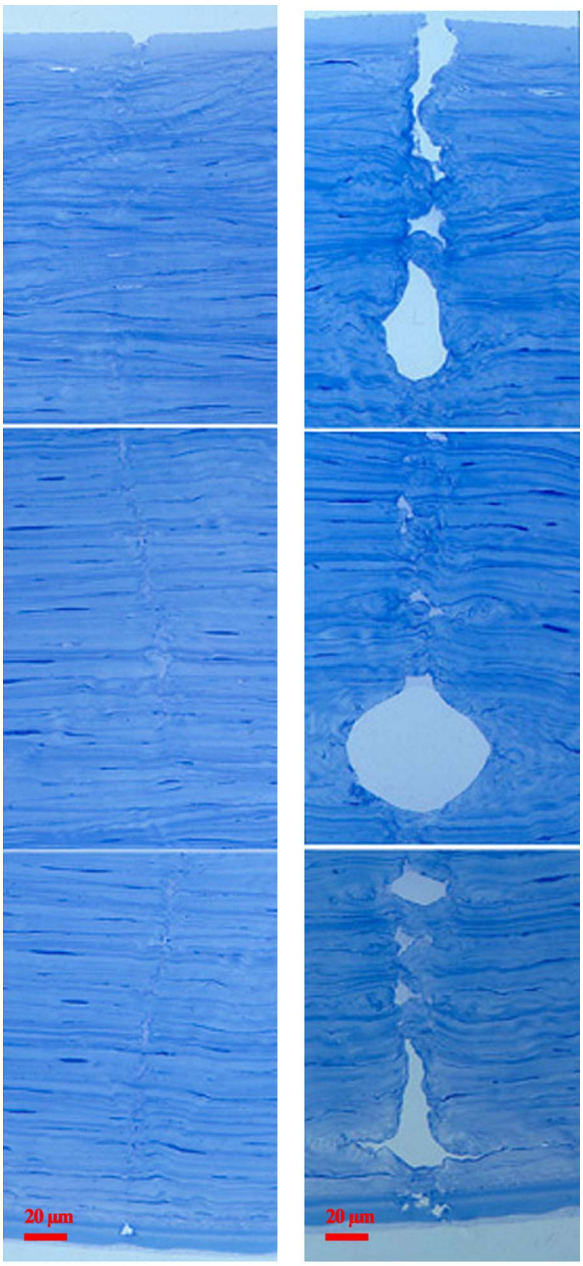

(a) (b)

Fig. 2 Histological section of a laser incision performed at NA=0.15, in a clear cornea, at constant energies of (a) 3 and (b) 5 μJ.

3.2 *Experiments on Clear Corneas at Varying NAs*

In a first step, incisions at constant pulse energies of 3 and 5 μJ were produced at NA=0.15 in fresh corneal tissue, which was free of edema. Incisions were performed by scanning the cornea under the beam in the axial direction, starting from the posterior region of the cornea. The selected scanning velocity provided a 2-μm spot separation. The left part of Fig. 2 shows a histological section of a transfixing cut performed at 3 μJ, slightly above the threshold. We can observe that the laser produced a regular incision of constant good quality across the depth of the cornea. This must be compared with the right part of Fig. 2, which depicts a laser incision

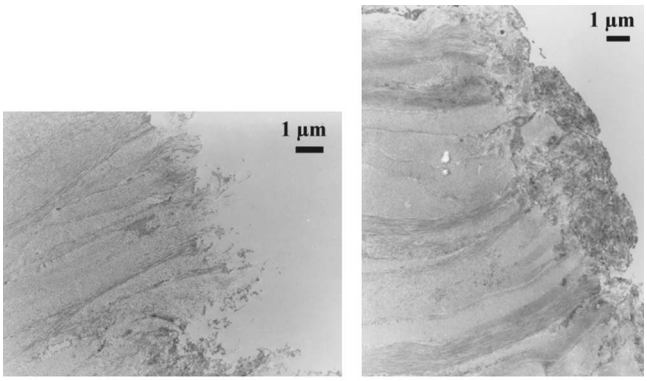

(a) (b)

Fig. 3 TEM micrographs of a laser incision in a clear cornea performed at NA=0.15 and constant energies of (a) 3 and (b) 5 μJ.

induced in the cornea by 5-μJ pulses. Although this energy corresponds to only about 2.5 times the experimental threshold energy, the resulting incision is considerably larger. Irregular residual cavities remain present in the corneal tissue with dimensions up to several tens of micrometers. The strong dependence of incision quality on laser energy is confirmed by an ultrastructural examination of the tissue. Figure 3 shows transmission electron microscope (TEM) pictures of the incision performed at 3 (left) and 5 μJ (right) in the anterior stroma. At 3 μJ, the region showing disorder in the collagen fibers at the edges of the cut extends only to micrometer depths in the tissue. In comparison, in the case of the 5-μJ incision, the perturbation of the collagen structure is more pronounced, and a hyperdensification of the collagen is visible at the borders of the incision corresponding to disordering and delamination effects.

From Fig. 4, note that comparable secondary effects may

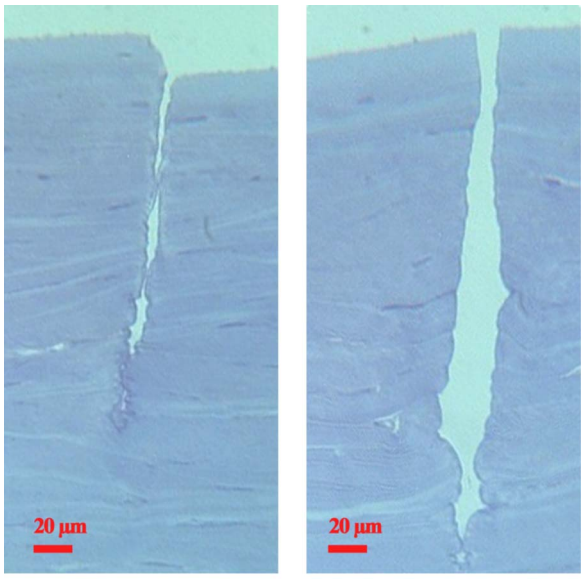

(a) (b)

Fig. 4 Histological section of a laser incision obtained with NA =0.75, in a clear cornea, at constant energies of (a) 250 and (b) 140 nJ.

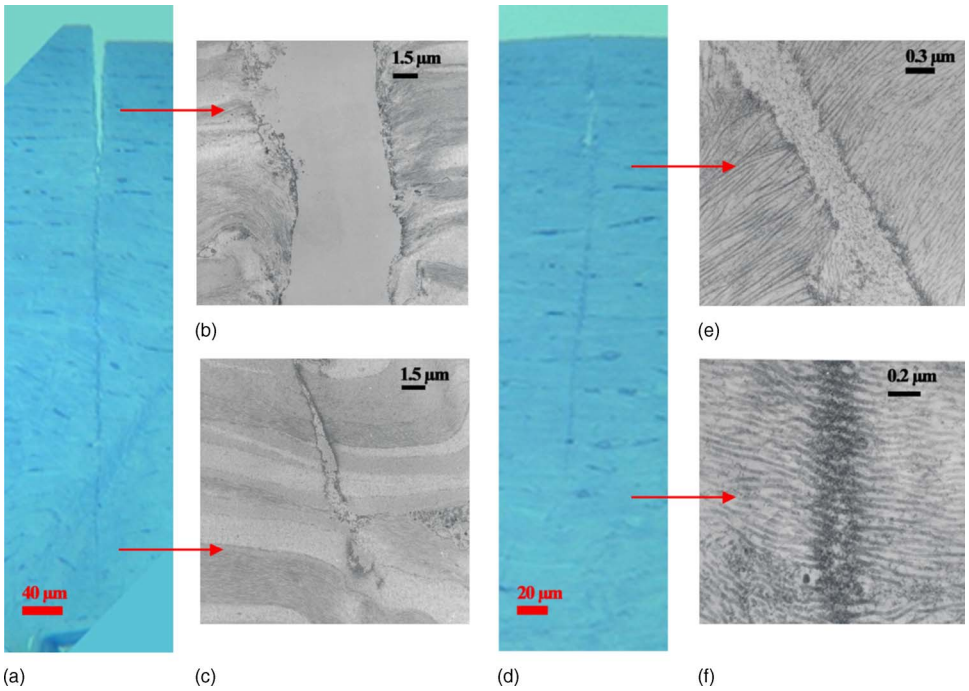

Fig. 5 (a) and (d) Histological sections of laser incisions in an edematous cornea performed at NA=0.3 and NA=0.5 and constant energies of 500 and 170 nJ, respectively; (b), (c), (e), and (f) TEM micrographs of the collagen in the anterior stroma (b) and (e) and at the end of the incision (c) and (f).

occur as well at high NAs when using an objective with NA=0.75. For these experiments, the alternative Ti:sapphire laser was used[†]. The incision on the right was made at moderate pulse energies of 140 nJ, which corresponds to about twice the experimental surface threshold. The cut is of good quality throughout the cornea depth. The incision on the left was obtained with pulse energies of 250 nJ—about 4 times the threshold—and shows in some places severe degradations of the tissue in the vicinity of the incision. However, in spite of the remaining side effects, the quality of the incisions obtained using NA=0.75 is, in both investigated cases, much better than in Fig. 2 for NA=0.15.

3.3 *Experiments on Edematous Cornea at Varying NAs*

In a second series of the experiments, performed at $\lambda = 800$ nm, laser surgery was performed in edematous corneas, in which the degree of organization of the collagen fibers is decreased and the amount of interstitial fluid is increased, thus reducing the transparency of the tissue and modifying its optical properties. Figure 5 shows histological and ultrastructural incisions made in the same pathological cornea with numerical apertures of 0.3 [Figs. 5(a) to 5(c)] and 0.5 [Figs. 5(d) to 5(f)], and at constant energies of 500 and 170 nJ, corresponding to roughly 2 times the threshold. We can notice that in edematous tissue, incisions performed at constant energies are of good quality in the anterior stroma but they are not penetrating. From the TEM micrographs, we can observe that in the anterior stroma, collagen fibers are properly disrupted and no secondary effects are visible. However, in the posterior stroma for keratoplasty at NA=0.3 and in the middle stroma for keratoplasty at NA=0.5, the incision becomes irregular and eventually ends at depths of about 500 (NA=0.3) and 280 μm (NA=0.5). Where the threshold for optical breakdown is not reached, a slight blackening of the tissue can be observed, which can be attributed to chemical alteration of the tissue occurring at radiant exposures slightly lower than the threshold. Obviously, although the incident pulse energy is kept constant, the laser beam broadening and attenuation due to the opacity of the tissue result in stronger disruption effects in the anterior part of the cornea than in the posterior region. As both incisions were performed at different NAs with equivalent parameters, a comparison of the laser penetration depths enables evaluating the influence of spherical aberration that occurs when the beam is focused from air into the volume of the cornea. At NA=0.3, the influence of spherical aberrations is small and the resulting penetration depth therefore mainly reflects the beam attenuation due to light scattering in the cornea. In this case, slightly augmenting the pulse energy enables us to perform transfixing incisions in mildly edematous corneas. In the case of NA=0.5, the penetration depth is reduced to less than 300 μm, which means that the spherical aberration contributes an additional attenuation of the same order of magnitude (see discussion for numerical simulations). Transfixing incisions in this cornea using this objective would require pulse energies of about 5 times the breakdown surface at the sample.

To further elucidate the influence of spherical aberrations, we performed additional experiments in which we used a mi-

[†]When comparing the results obtained with the two different lasers, strictly speaking we should take into account that the shorter wavelength of the Ti:sapphire laser corresponds to a slightly lower critical power for the onset of filamentation processes, and that the shorter pulse duration corresponds to a slightly lower theoretical threshold for optical breakdown.

Fig. 6 Histological section of laser incisions in an edematous cornea performed at NA=0.6 with correction of spherical aberrations at depths of 300, 450, and 640 μm, respectively (from left to right).

croscope objective specifically designed to correct spherical aberrations in the volume of the tissue for a given depth. Figure 6 shows incisions performed at NA=0.6 in a strongly edematous cornea with corrections at depths of 300, 450, and 640 μm, respectively (from left to right), using energies of 4 times the surface threshold and yielding incision depths of about 280, 320, and 200 μm. We see from comparing the second to the first incision that correcting for an increased depth in the sample results in an increased incision length. However, moving the corrected plane too far from the interaction region in scattering tissues, as was done for the third incision, decreases the beam quality, and the overall incision length is reduced.

3.4 *Lamellar Incisions at Varying NAs*

In addition to the preceding experiments, lamellar incisions were performed in the anterior stroma of edematous cornea using focusing optics with varying numerical apertures. Lamellar cuts enable the observation of self-focusing effects, as in this geometry they are perpendicular to the incision plane. These experiments were performed with the Ti:sapphire laser. Figures 7(a) to 7(c) illustrate histological sections of incisions induced at 150 μm from the corneal surface with NA=0.3 and 0.5 at energies of 900 and 450 nJ, which correspond to about 3 times the threshold determined experimentally. The quality of the incisions improves greatly with increasing numerical aperture. Self-focusing effects are still visible in the histological sections for NA=0.3 and, to a smaller extent, for NA=0.5. Figures 7(a) and 7(d), present the histological section of the incision performed at NA=0.75 at a pulse energy of 150 nJ (about 2.5 times the experimental threshold), showing little secondary effects. The general tendency of these observations is confirmed by ultrastructural imaging using TEMs [Figs. 7(e) to 7(g)], which show streak

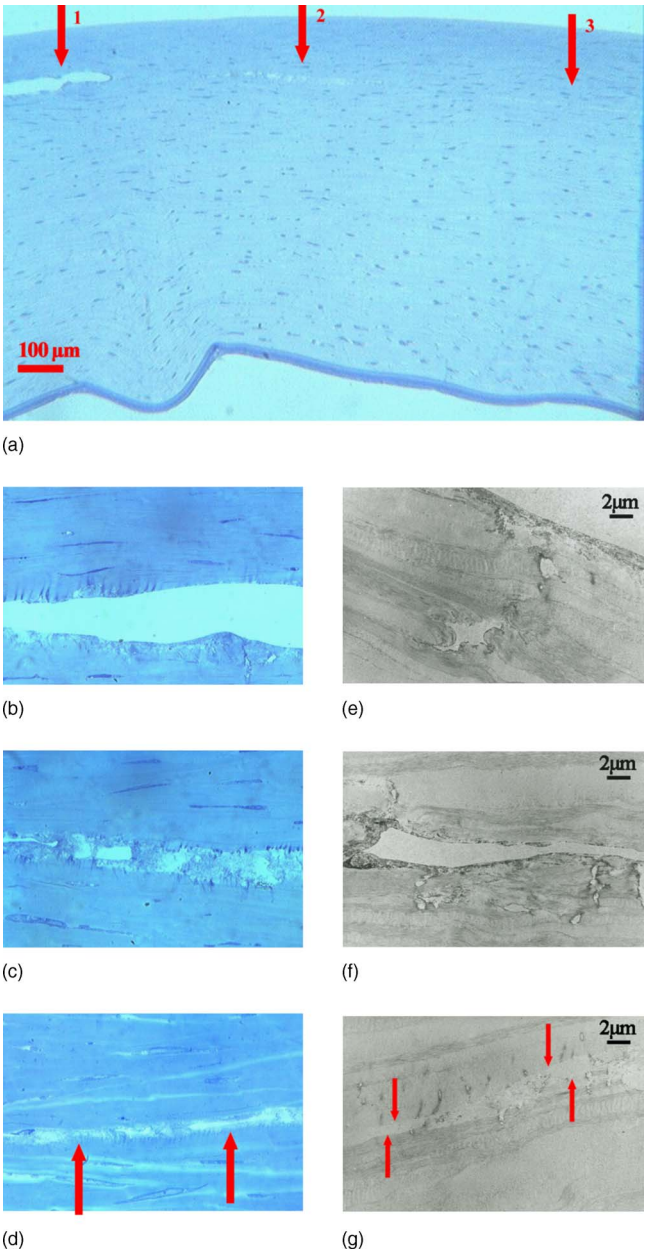

Fig. 7 Histological section of lamellar laser incisions induced at 150 μm from the corneal surface with NA=0.3 (a1) and (b), 0.5 (a2) and (c), and 0.75 (a3) and (d) at energies of 900, 450, and 150 nJ, respectively; (e) to (g) detail of the lamellar incisions from TEMs at NA=0.3, 0.5, and 0.75, respectively.

formation and residual cavities. The strength of this effect diminishes with increasing NA, but it remains present even at NA=0.75.

3.5 *"Optimal" NA*

A question may arise as to what the "optimal" NA for femtosecond corneal surgery in the entire volume of the cornea should be. We already observed that intermediate NAs enable us to considerably reduce the pulse energy compared to low NAs, while improving the quality of the incision. Low NAs (NA$<$0.3) are not advisable for other reasons as well: for very strongly scattering tissue (sclera, skin, very strongly

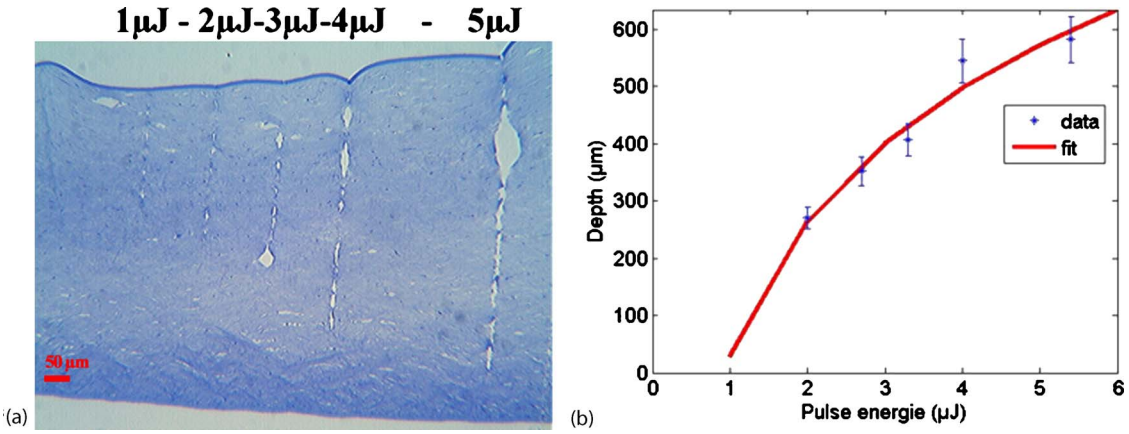

Fig. 8 (a) Histological section of laser incisions performed at energies of 1, 2, 3, 4, and 5 μJ with NA=0.15 and (b) penetration depth of the laser versus laser power. The red line represents the fitting curve. (Color online only.)

opacified cornea), the superficial radiant exposure may even be higher than in the focal plane.[38] Where high NAs are concerned, an upper limit is more difficult to give. Very high NAs—as used in cell nanosurgery—enable us to reduce pulse energies to the nanojoule range; however, they require a high-repetition-rate laser because the small bubble size would otherwise result in prohibitive durations for the procedure and a good correction for spherical aberrations using adaptive optics and/or working in immersion, which might be arduous in clinical practice. Furthermore, the small field of view does not enable us to use a beam scanning system for the entire surface of the cornea and does not enable visual control of the operation by the surgeon. Objectives without immersion typically reach maximum NAs of 0.75. At these high values, the influence of spherical aberration in the volume of the cornea is strong, the field of view is limited, and the working distance is generally small; they are therefore not adapted for a use in surgery. Depending on the requirements of the actual system, a compromise between small pulse energy, side effect reduction, bubble size, field of view, working distance, and other constraints must be made. "Optimal" NAs for a use in clinical practice will therefore probably lie in the range of 0.4 to 0.6.

3.6 *Quantification of the Laser Beam Attenuation by Histology*

For a systematic quantification of the laser beam attenuation, in a first step, the penetration depth of the laser beam as a function of pulse energy was studied for the case of a typical edematous cornea. Incisions were induced using NA=0.15 and pulse energies of 1 to 5 μJ in 1-μJ steps. Figure 8(a) shows the histological section of the cornea after laser treatment. The laser incisions corresponding to the different energies are clearly visible and the incision length increases with increasing pulse energy. The relation of maximum incision depth to pulse energy is plotted in Fig. 8(b). As expected for the case of exponential attenuation of the beam, a logarithmic dependence of the incision length as a function of the necessary pulse energy is observed. A logarithmic regression yielded a 1/*e* penetration depth of 342±30 μm for this particular cornea. It is not necessary to generalize this result; the penetration depth of the laser beam in edematous cornea varies considerably with the degree of the edema and is also slightly dependent on the position on the specimen. To be able to compensate for the attenuation in *in vivo* surgical procedures, this parameter should be determined for each cornea under treatment, therefore requiring an *in situ* nondestructive method.

3.7 *Nondestructive Optical Quantification of the Laser Beam Attenuation*

To quantify the radiant exposure at the focal volume of the laser beam as a function of the depth coordinate in the cornea, we make use of the backscattered frequency-doubled light that is created due to the nonlinear properties of the tissue. Experiments were performed at energies well below the threshold for optical breakdown. The focusing of the laser was achieved with the 20× objective, NA=0.5, corresponding to a configuration used in clinical practice. The focal spot of the laser was scanned through the cornea in 10-μm steps in the laser beam direction from the endothelium toward the corneal surface while recording the generated second harmonic signal. The axial coordinates of the surface of the cornea were determined by measuring the position at which the peak in the SHG signal corresponding to the coverslip/cornea interface was observed. As corneas produced the SHG signal across their entire volume, their thickness was determined by measuring the position of the drop in the SHG signal at their rear surface. The numerical value of the thickness was obtained by correcting the difference between surface and rear surface position by the projection factor of the focal volume into the cornea using a value of 1.4 for its refractive index.

Since the strength of the SHG signal is proportional to the square of the incident radiant exposure, the measurement of the backscattered second-harmonic (SH) signal enables us to quantify the laser beam radiant exposure at the focal volume. Figure 9 presents a graph of the SH radiation versus the corneal depth obtained in our experiments. The SH signal is normalized with respect to the measured SH generated at the surface. SH emission acquired from the endothelium toward the epithelium showed an approximately exponential attenuation, when illuminating the sample at constant pulse energy below the ablation threshold.

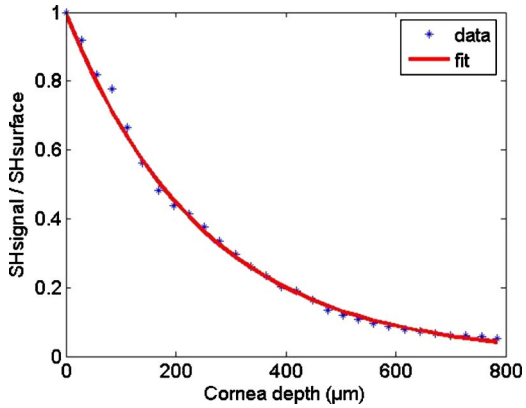

Fig. 9 Attenuation of the backscattered SHG emission in a cornea irradiated by the Nd:glass laser at a nondestructive energy.

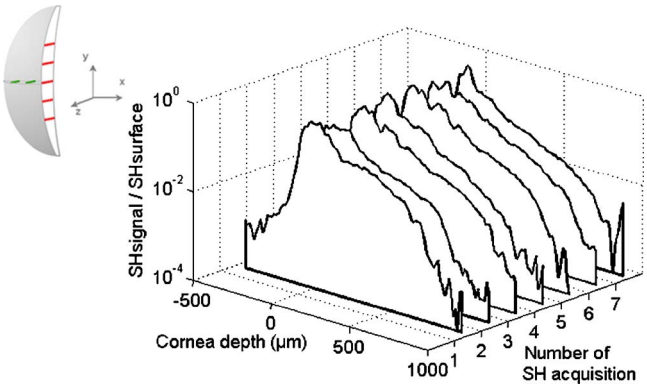

Fig. 10 Attenuation of the SH signal in the volume of an individual cornea at different lateral coordinates.

The variation of the SHG as a function of the depth coordinate z and consequently the attenuation of the laser can be expressed by the relation

$$I_{\mathrm{SH}} = \left[I_0 \exp\left(-\frac{z}{l} \right) \right]^2 e^{-\mu z},$$

where I_0 is the incident laser intensity, l is the $1/e$ penetration depth of the laser in the cornea at the incident wavelength of 1.06 μm, and μ is the corneal attenuation coefficient for the frequency-doubled light traveling back to the surface. For the purpose of the presented work it proved to be sufficient to assume l as a constant and that the μ coefficient is negligible. The latter simplification means that the attenuation of the SHG is neglected and that the exponential decrease of the SH emission as a function of the depth is exclusively due to the attenuation or broadening of the laser. This approach relies on the assumption that in our backscattering geometry, multiply scattered SHG photons are detected on a large surface detector, the collective intensity of which does not depend much on the depth of the focal volume in the cornea where they are created.

On a series of 10 corneas presenting edema of varying degree, measurements of the type presented in Fig. 9 were performed at different lateral coordinates and the $1/e$ penetration lengths were calculated using a linear regression algorithm of the logarithm of the measured values. The penetration depths may vary with the position on the cornea. Pathological corneas are typically slightly inhomogeneous: by evaluating the SH emission at different positions, it is possible to establish a 3-D cartography of the local attenuation of the cornea. Figure 10 shows the attenuation of the SH signal in the volume of an individual cornea at different lateral coordinates. The average $1/e$ penetration lengths of the entire group of edematous corneas tested are compiled in Table 2. Depending on the degree of edema, the thickness of the corneas varied between 600 and 1100 μm and values between 200 and 400 μm were calculated for the laser penetration depths. The ratio of thickness to penetration depth varied from 1.8 for the weakly edematous cornea 4 to 3.8 for the strongly edematous cornea 2.

3.8 *Compensating for the Laser Beam Attenuation*

The values obtained for the laser penetration depth can be used to correct the energy reduction in the depth of the sample. Figure 11 presents an incision made in a pathological cornea with a measured penetration depth of 350±20 μm. The incision was performed with the achromatic doublet lens; the pulse energies varied from 2 at the surface to about 5 μJ in the volume, corresponding to the maximum pulse energy available, which was reached at a depth of about 320 μm. Note that no unwanted side effects are visible in vicinity of the incision in the anterior stroma and that the incision is of uniform quality (except for a slightly extended ablation zone at the surface of the cornea). However, the maximal available energy limited the incision depth to about half of the cornea. It can in fact easily be calculated from the preceding values that a transfixing incision would have required about 6 times the energy corresponding to the threshold at the surface.

4 Discussion and Perspectives

The experiments concerning perforating femtosecond laser incisions in clear corneal tissue at threshold radiant exposure and above show significant histological differences. The laser cuts induced close to the threshold exhibited only localized

Table 2 Measure of the $1/e$ penetration depth of the laser in the volume of 10 corneas.

Cornea	1	2	3	4	5	6	7	8	9	10
Thickness (μm)	700	750	850	600	900	750	800	1100	1000	1000
Penetration length (μm)	205	210	299	313	326	337	359	381	388	476
Standard deviation (μm)	13	13	22	27	24	23	32	28	27	29

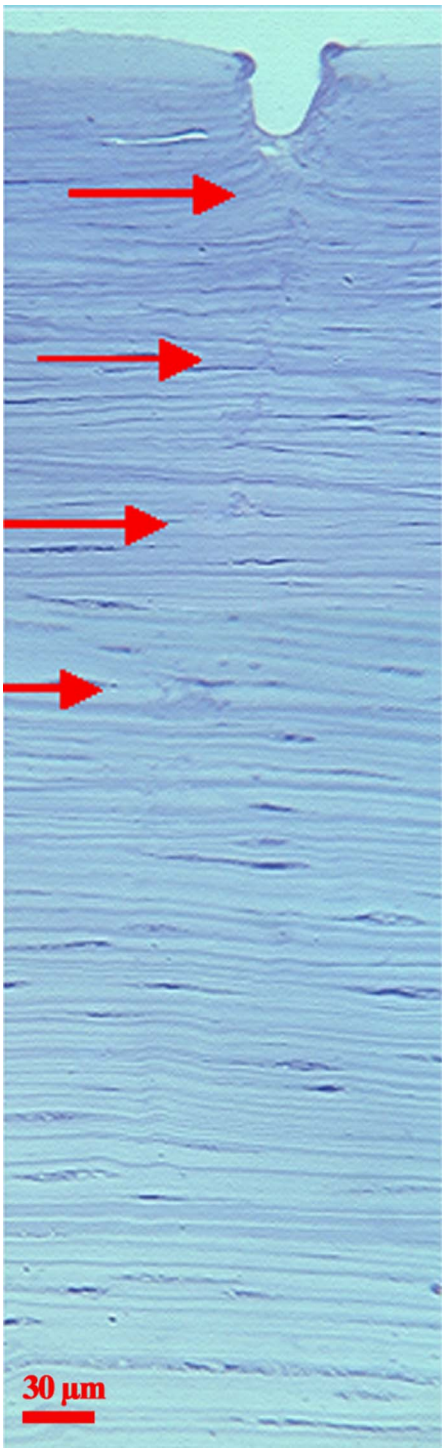

Fig. 11 Incision in the anterior and middle stroma performed with NA=0.15 and laser pulse energies varying from 2 to 5 μJ.

disorganization of the stroma, whereas the incisions induced at higher energies presented a strong disorder of the stroma, the consequence of which may be diffuse lamellar keratisis. These side effects were reduced, but not suppressed, by focusing the beam with a high NA.

When performing transfixing incisions in edematous cornea at NA$\geq$0.3, the additional effect of beam attenuation by optical scattering and aberrations becomes manifest and must be taken into account. When attempting to maximize incision depths by using moderate higher constant laser energy, the anterior stroma does not show any disorder of the collagen, however, the fibers in the posterior stroma are no longer disrupted or low density plasma chemical effects can produce permanent modification of the tissue. Experiments performed with correction of spherical aberration at a fixed depth exhibit that aberrations can be corrected until a maximum optimal depth, which depends on the scattering contribution to the attenuation and which in edematous tissue may be lower than the total thickness of the cornea. The series of lamellar incisions reveal the formation of filamentation along the axis of the laser beam and confirm the expected reduction of secondary effects with increasing numerical aperture and optimized energy.[39]

A posteriori histological analysis of cornea incisions obtained with varying pulse energies offers a straightforward but destructive means to quantify the laser beam penetration depth. To good approximation, maximum incision depths showed logarithmic dependence on pulse energies consistent with a simple Lambert-Beer exponential behavior.

This was confirmed by the noninvasive attenuation measurements by SHG. Penetration depths between l=200 μm and l=400 μm could be measured in edematous cornea. We performed numerical calculations using the ZEMAX program[33] to assess the contributions of scattering and of focus enlargement by spherical aberrations to the reduction of irradiance with depth. It turned out that the irradiance reduction by spherical aberrations equals the attenuation in an absorbing system with $1/e$ optical penetration depth of roughly $l_{sa}\approx 800$ μm. If we estimate the penetration depth due to scattering as $l_{sc}\approx(1/l-1/l_{sa})^{-1}$, we obtain minimal and maximal values of $l_{sc}\approx 270$ and $l_{sc}\approx 800$ μm for the scattering penetration depth. In the first case, optical scattering by the modified structure of the collagen matrix of the cornea is the most prominent process contributing to the attenuation of the radiant exposure. In the latter case, corneas can be considered only slightly edematous and therefore relatively transparent; scattering and beam broadening due to spherical aberrations contribute equally. Corneas corresponding to even higher degrees of transparency did not produce sufficient backscattering to enable the determination of the optical penetration depth, which led us to believe that these corneas do not require a depth-dependent correction of the pulse energy. Note that the experimentally determined penetration depth l represents the combined effects of all processes contributing to radiant exposure reduction. It is therefore this value that is used for the correction of the energy and it could be demonstrated that laser incisions performed with energy correction in the volume of pathological cornea showed uniform good quality throughout the depth of the incision.

When conceiving future systems we must consider that the reserve energy necessary to perform perforating cuts in strongly scattering corneas can reach considerable levels and standard clinical femtosecond-laser setups must be adapted accordingly. Future systems should also address and compensate for the physical mechanisms of the beam attenuation. The implementation of a deformable mirror in a system for the correction of spherical aberrations would preserve the quality of the beam in the volume of the cornea. Scattering and self-

focusing effects will be greatly reduced by shifting laser system wavelengths farther into the IR, probably in the optical window between the two water absorption peaks at 1.5 and 1.9 μm. The scattering mechanisms—be they Rayleigh or Mie scattering—are strongly reduced at longer wavelengths,[40] and conditions concerning self-focusing and filamentation become less critical as the critical power for their onset grows with the square of the wavelength.[9]

Acknowledgments

We gratefully acknowledge Dr. Patrick Sabatier of the Banque Française des Yeux (French Eye Bank) for the supply of the human corneas.

References

1. T. Juhasz, F. H. Loesel, C. Horvath, R. M. Kurtz, and G. Mourou, "Corneal refractive surgery with femtosecond lasers," *IEEE J. Sel. Top. Quantum Electron.* **5**, 902–910 (1999).
2. A. Heisterkamp, T. Mamom, W. Drommer, W. Ertmer, and H. Lubatschowski, "Photodisruption with ultrashort laser pulses for intrastromal refractive surgery," *Laser Phys.* **13**, 743–748 (2003).
3. L. T. Nordan, S. G. Slade, R. N. Baker, C. Suarez, T. Juhasz, and R. J. Kurtz, "Femtosecond laser flap creation for laser in situ keratomileusis: six-month follow-up of initial U.S. clinical series," *J. Refract. Surg.* **19**, 8–14 (2003).
4. G. M. Kezirianx and K. G. J. Stonecipher, "Comparison of the IntraLase femtosecond laser and mechanical keratomes for laser in situ keratomileusis," *J. Cataract Refractive Surg.* **30**, 804–811 (2004).
5. B. Seitz, A. Langenbucher, C. Hofmann-Rummelt, U. Schlotzer-Schrehardt, and G. O. Naumann, "Nonmechanical posterior lamellar keratoplasty using the femtosecond laser (femto-plak) for corneal endothelial decompensation," *Am. J. Ophthalmol.* **136**, 769–772 (2003).
6. H. K. Soong, S. Mian, O. Abbasi, and T. Juhasz, "Femtosecond laser-assisted posterior lamellar keratoplasty: initial studies of surgical technique in eye bank eyes," *Ophthalmology* **112**, 44–49 (2005).
7. A. Vogel, K. Nahen, D. Theisen, R. Birngruber, R. J. Thomas, and B. A. Rockwell, "Influence of optical aberrations on laser-induced plasma formation in water and their consequences for intraocular photodisruption," *Appl. Opt.* **38**, 3636–3643 (1999).
8. Z. S. Sacks, R. M. Kurtz, T. Juhasz, G. Spooner, and G. Mourou, "Subsurface photodisruption in human sclera: wavelength dependence," *Ophthal. Surg. Lasers Imag.* **4**, (2), 104–113 (2003).
9. C. L. Arnold, W. Ertmer, and H. Lubatschowski, "Modeling of ultrashort pulse propagation and nonlinear plasma formation in transparent Kerr media using realistic initial conditions," *Proc. SPIE* **6460**, 646010 (2007).
10. A. Couairon and A. Mysyrowicz, "Femtosecond filamentation in transparent media," *Phys. Rep.* **441**, 47–189 (2007).
11. A. Heisterkamp, T. Ripken, T. Mamom, W. Drommer, H. Welling, W. Ertmer, and H. Lubatschowski, "Nonlinear side effects of fs pulses inside corneal tissue during photodisruption," *Appl. Phys. B* **74**, 419–425 (2002).
12. D. Strickland and G. Mourou, "Compression of amplified chirped optical pulses," *Opt. Commun.* **55**, 447–449 (1985).
13. P. F. Moulton, "Spectroscopic and laser characteristics of Ti: Al2O3," *J. Opt. Soc. Am. B* **3**, 125–133 (1986).
14. D. Kopf, F. X. Kartner, U. Keller, and K. J. Weingarten, "Diode-pumped mode-locked Nd:glass lasers with an antiresonant Fabry-Perot saturable absorber," *Opt. Lett.* **20**, 1169–1171 (1995).
15. A. Vogel, S. Busch, K. Jungnickel, and R. Birngruber, "Mechanisms of intraocular photodisruption with picosecond and nanosecond laser pulses," *Lasers Surg. Med.* **1**, 32–43 (1994).
16. D. B. Brown, W. J. O'Brien, and R. O. Schultz, "Corneal ablations produced by the neodymium doped yttrium-lithium-fluoride picosecond laser," *Cornea* **13**, 471–478 (1994).
17. A. Vogel and V. Venugopalan, "Mechanisms of pulsed laser ablation of biological tissues," *Chem. Rev. (Washington, D.C.)* **103**, 577–644 (2003).
18. A. Vogel, J. Noack, G. Hüttman, and G. Paltauf, "Mechanisms of femtosecond laser nanosurgery of cells and tissues," *Appl. Phys. B* **81**, 1015–1047 (2005).
19. A. P. Joglekar, H. H. Liu, G. J. Spooner, E. Meyhöfer, G. Mourou, and A. J. Hunt, "A study of the deterministic character of optical damage by femtosecond laser pulses and applications to nanomachining," *Appl. Phys. B* **77**, 25–30 (2003).
20. A. P. Joglekar, H. H. Liu, E. Meyhöfer, G. Mourou, and A. J. Hunt, "Optics at critical intensity: applications to nanomorphing," *Proc. Natl. Acad. Sci. U.S.A.* **101**, 5856–5861 (2004).
21. J. Noack and A. Vogel, "Laser-induced plasma formation in water at nanosecond to femtosecond time scales: calculation of thresholds absorption coefficients and radiant exposure," *IEEE J. Quantum Electron.* **35**, 1156–1167 (1999).
22. A. Vogel, J. Noack, K. Nahen, D. Theisen, S. Busch, U. Parlitz, D. X. Hammer, G. D. Noojin, B. A. Rockwell, and R. Birngruber, "Energy balance of optical breakdown in water at nanosecond to femtosecond time scales," *Appl. Phys. B* **68**, 271–280 (1999).
23. V. Keldysh, "Ionization in the field of a strong electromagnetic wave," *Sov. Phys. JETP* **20**, 1307–1314 (1965).
24. S. Fine and W. P. Hansen, "Optical second harmonic generation in biological system," *Appl. Opt.* **10**, 2350–2353 (1971).
25. R. M. Williams, W. R. Zipfel, and W. W. Webb, "Interpreting second-harmonic generation images of collagen I fibrils," *Biophys. J.* **88**, 1377–1386 (2005).
26. K. Plamann, O. Albert, D. Giulieri, D. Donate, F. May, J. M. Giraud, and J. M. Legeais, "In situ multiphoton microscopy for monitoring femtosecond laser eye surgery in the human cornea and sclera," *Proc. SPIE* **5860**, 1–7 (2005).
27. A. Zoumi, A. T. Yeh, and B. J. Tromberg, "Imaging cells and extracellular matrix in vivo by using second-harmonic generation and two-photon excited fluorescence," *Proc. Natl. Acad. Sci. U.S.A.* **99**, 11014–11019 (2002).
28. D. Debarre, A. M. Pena, W. Supatto, T. Boulesteix, M. Strupler, M. P. Sauviat, J. L. Martin, M. C. Schanne-Klein, and E. Beaurepaire, "Second- and third-harmonic generation microscopies for the structural imaging of intact tissues," *Med. Sci. (Paris)* **22**, 845–852 (2006).
29. M. Han, G. Giese, M. Walter, F. H. Loesel, and J. F. Bille, "Second-harmonic imaging of cornea after intrastromal femtosecond laser ablation," *J. Biomed. Opt.* **9**, 760–766 (2004).
30. S. W. Teng, H. Y. Tan, J. L. Peng, H. H. Lin, K. H. Kim, W. Lo, Y. Sun, W. C. Lin, S. J. Lin, S. H. Jee, P. T. So, and C. Y. Dong, "Multiphoton autofluorescence and second-harmonic generation imaging of the ex vivo porcine eye," *Invest. Ophthalmol. Visual Sci.* **47**, 1216–1224 (2006).
31. M. Mueller, M. Han, G. Giese, J. F. Bille, and M. H. Niemz, "Revealing the structural disorder of the keratoconic cornea with second harmonic generation microscopy," in *Proc. ARVO Annual Meeting*, abstract 2994-B94 (2006).
32. P. J. Campagnola and L. M. Loew, "Second-harmonic imaging microscopy for visualizing biomolecular arrays in cells, tissues and organisms," *Nat. Biotechnol.* **21**, 1356–1360 (2003).
33. ZEMAX EE, Optical Design Program, ZEMAX Development Corporation (1999).
34. Vogel, A., Institute of Biomedical Optics, University of Lübeck, Private Communication.
35. M. H. Niemz, T. Hoppeler, T. Juhasz, and J. F. Bille, "Threshold fluence measurements for plasma-mediated ablation in corneal tissue. Laser pulse duration was between 120 fs and 100 ps," *Laser Light Ophthalmol.* **5**, 149–155 (1993).
36. B. C. Stuart, M. D. Feit, S. Herman, A. M. Rubenchik, B. W. Shore, and M. D. Perry, "Nanosecond-to-femtosecond laser-induced breakdown in dielectrics," *Phys. Rev. B* **53**, 1749–1761 (1996).
37. D. Giguère, G. Olivié, F. Vidal, S. Toetsch, G. Girard, T. Ozaki, J. C. Kieffer, O. Nada, and I. Brunette, "Laser ablation threshold dependence on pulse duration for fused silica and corneal tissue: experiments and modeling," *JOSA A* **24**, 1562–1568 (2007).
38. J. Q. Lu, X.-H. Hu, and K. Dong, "Modeling of the rough-interface effect on a converging light beam propagating in a skin tissue phantom," *Appl. Opt.* **39**, 5890–5897 (2000).
39. K. Koenig, O. Krauss, and I. Riemann, "Intratissue surgery with 80 MHz nanojoule femtosecond laser pulses in the near infrared," *Opt. Express* **10**, 171–176 (2002).
40. J. R. Mourant, T. Fuselier, J. Boyer, T. M. Johnson, and I. J. Bigio "Predictions and measurements of scattering and absorption over broad wavelength ranges in tissue phantoms," *Appl. Opt.* **36**, 949–957 (1997).